VOL. 20, NO. 10, MAY 2025 ISSN 1819-6608
ARPN Journal of Engineering and Applied Sciences

www.arpnjournals.com

PERFORMANCE COMPARISON ANALYSIS OF ARTIFICIAL NEURAL NETWORK (ANN) AND ADAPTIVE NEURO-FUZZY INFERENCE SYSTEM (ANFIS) FOR INTELLIGENT MANAGEMENT OF DISTRIBUTED GENERATION

Alias Khamis[1], Gan Chin Kim[1], Mohd Shahrieel Mohd Aras[1], Nor Aira Zambri[2] and Zairi Ismael Rizman[3]
[1]Faculty of Electrical Technology and Engineering, Universiti Teknikal Malaysia Melaka, Malaysia
[2]Faculty of Electrical and Electronic Engineering, Universiti Tun Hussein Onn Malaysia, Malaysia
[3]School of Electrical Engineering, College of Engineering, Universiti Teknologi MARA, Terengganu, Malaysia
E-Mail: alias@utem.edu.my

ABSTRACT

To control the voltage source inverter (VSI) of the PV/Fuel Cell/Battery cell system, conventional methods of controlling voltage and current modes were developed with improved controllers of the proportional Integral (PI) Neural Network (NN) of both the output voltage and the internal current control loop. The suggested neural network PI controller performs better than the adaptive neurofuzzy inference system (ANFIS) controller while maintaining the PI controller's reliability and ease of use. VSI controllers have employed space vector type pulse width modulation to produce sine-shaped waves. The proposed inverter-based Distributed Generation (DG) model is applied to the micro-grid-system to review its effectiveness as a complete model as well as to evaluate the performance of its use in large network systems. Since the VSI model is built on a P-Q control scheme that allows separate control of active and reactive power output, DG can operate based on active and reactive power references on the inverter. A new technique has been developed to manage active and reactive power reference for DG by using an ANN to ensure that the DG unit operates at optimal power values while reducing the amount of power loss, as well as maintaining the voltage profile within acceptable limits. The results showed that the proposed artificial NN technique could accurately predict the active and reactive power references of DG with minimal error. A comparison was made between the ANFIS DG-logic controller and the NN PI controller for the VSI in terms of the generation of evaluation metrics.

Keywords: artificial neural network, adaptive neuro-fuzzy inference system, distribution generation, microgrid.

Manuscript Received 14 November 2025; Revised 14 May 2025; Published 5 August 2025

INTRODUCTION

Depletion of fossil fuel and growing awareness of environmental issues, renewable energy sources (RES) such as wind, solar radiation, microturbine (MT), fuel cell (FC), and battery energy storage (BES) with low emission of pollutant gases are becoming more attractive [1, 2, 3]. In line with the growing environmental concerns, the Malaysian government has taken a proactive action in facilitating the growth of RES in the national power generation mix. This has been proven by the several measures taken so far, such as the Fifth-Fuel Policy under 8th and 9th Malaysia Plan, The Kyoto Protocol, the Malaysian Building Integrated Photovoltaic (MBIPV) Programme and Biomass [4][5] and with the latest Renewable Energy Act and Action Plan [6, 7, 8, 9]. Even though RES is receiving a lot of attention due to the fact that it causes little or no environmental damage, it is unreliable due to its intermittent nature [10, 11, 12].

For maintaining reliability of the electricity supply, green energy resources such as MT, FC, and BES should be taken into account as a mix of energy resources because these resources are the greenest and cleanest technologies after wind and solar [13, 14, 15]. These technologies are seen as electrical energy sources that could fill the gap between environmentally unfriendly conventional power plants and pollution-free power plants powered by RES. A combination of two or more RES power generation technologies will optimize their operating characteristics and increase efficiencies more than that obtained from a single power source [16][17]. In addition, advances in power electronics technologies facilitate the integration of various RES.

In conventional power systems, the synchronous generators (SG) are usually located far from the load centers and are centrally controlled. By integrating the new RE-based generation technologies in a power system, the generators are distributed, located near the load, and have different characteristics compared to the conventional SG. As the traditional power system development is influenced by the characteristics of SG, the integration of distributed generation (DG) into the existing power network on a large scale is expected to create many technical and operational challenges [18, 19, 20, 21]. A thorough study needs to be performed to assess various operational aspects to identify problems that may arise and to find the best countermeasures that can be taken. Before these important studies can be done, accurate dynamic models of RE resources need to be developed. Synchronous generators (SG) are often dispersed from load centres and centrally regulated in conventional power networks. The generators are distributed, situated close to the load centers, and have distinct properties when

compared to the traditional SG when the new RE-based generation technologies are integrated into a power system. Large-scale integration of distributed generation (DG) into the current power network is anticipated to provide numerous technical and operational difficulties because the evolution of the traditional power system is influenced by the characteristics of SG [22]. It is necessary to do a thorough analysis of the many operational components in order to pinpoint potential issues and choose the best preventative actions. Accurate dynamic models of RE resources must be created before this crucial research can be carried out [23].

Small non-conventional generation combined with renewable energy-based distributed generation (REDG), like wind-electric conversion systems, photovoltaic systems, is rapidly emerging for electric power generation. Furthermore, the low power generation capacity of renewable and green energy sources has motivated the need for integration of different types of REDGs and loads in the form of a microgrid to enhance power generation capacity, reliability, and marketability of dispersed types of microsources [24]. A microgrid is normally interfaced with the load and utility grid by power electronic inverters. It can operate in grid-connected mode or islanded mode. In grid-connected mode, the microgrid either draws or supplies power from or to the main grid, depending on the generation and load. On the other hand, the microgrid should disconnect itself from the main grid upon the occurrence of an abnormal condition and has to be shift to islanded mode, and a balanced condition is to be maintained between supply and demand applicable to the microgrid [25][26]. However, a microgrid has no spinning reserves like in the normal power grid system. Most microsources have a delayed response when implementing secondary voltage and frequency control. For this reason, if the microgrid is exchanging power with the grid before disconnection, then secondary control actions should be applied to balance generation and consumption in islanded mode to ensure initial balance after a sudden fluctuation in load or generation. The intermediate storage units and microsources with built-in battery banks are normally used as spinning reserves. Considering the above factors, a microgrid should be prepared for grid connected and islanded modes of operation to maintain continuity of power supply.

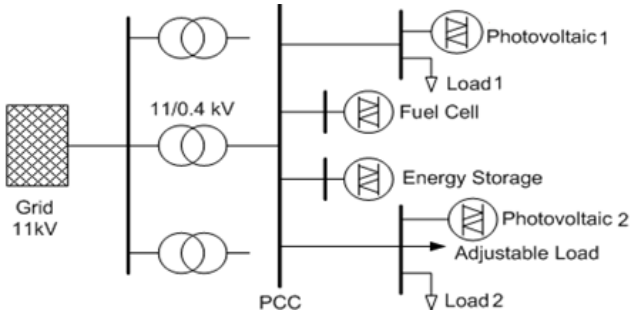

Figure-1. Single line diagram of the AC microgrid.

METHODOLOGY

Active and Reactive Power Controls in Distribution Systems.

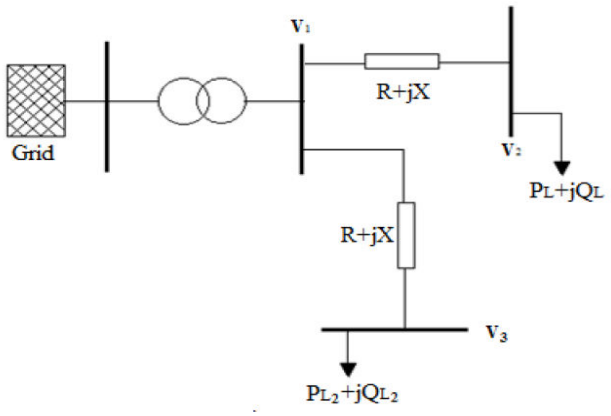

Figure-2. A simple radial power system illustrating voltage drop.

The basic concept of power losses is explained through the single line diagram of a simple radial power system shown in Figure-2. In a simple radial system, the voltage drop along the feeder is given by the following equation [8]:

$$V_1 - V_2 \approx \frac{RP_L + XQ_L}{V_2}, \quad (1)$$

Where R and X are the resistance and reactance of the line, respectively, and PL and QL are the active and reactive load powers, respectively.

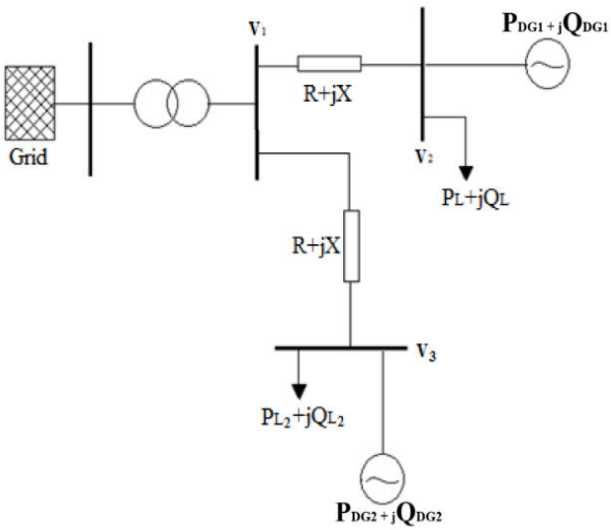

Figure-3. A simple radial power system with a DG unit.

The equation shows that the load always results in a voltage drop in the conventional distribution systems, and hence, it increases the total loss in the system. Active

and reactive power demands are compensated for by adding a DG unit to a network, which will be connected to a load bus as shown in Figure-3. This process will boost the voltage profile and reduce the voltage drop in the feeder, which is given by,

$$V_1 - V_2 \approx \frac{R(P_L - P_{DG}) + X(Q_L - Q_{DG})}{V_2}, \quad (2)$$

Where PDG and QDG are the active and reactive powers injected into the feeder by the DG unit, respectively. When a DG unit compensates the active and reactive power demand, the current flowing through a network will decrease, and it is given by,

$$I = \frac{\sqrt{(P_L - P_{DG})^2 + (Q_L - Q_{DG})^2}}{V_2}, \quad (3)$$

Therefore, the total feeder loss, Ploss, will also decrease because power losses are proportionally related to the magnitude of the current flowing through the resistance line. The feeder loss is given by,

$$P_{loss} = I^2 R. \quad (4)$$

To properly compensate for the active and reactive power demand that changes with every change of load, the DG unit is required to supply optimal active and reactive powers depending on the variation of the load. For a system with more than one DG unit, coordination between the DG units is needed.

Inverter Based Distributed Generation

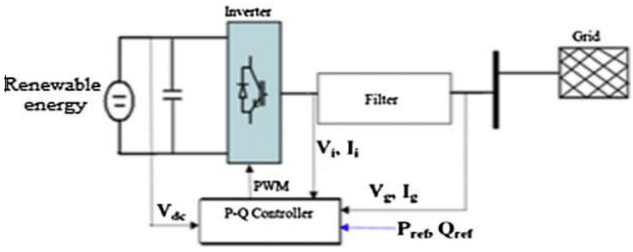

Figure-4. Renewable energy technology with a voltage source inverter.

In order to integrate with the utility grid, distributed generation using renewable and green energy technology, such as PV, FC, micro-turbines, and energy storage systems, produces DC electrical power that must be converted to AC form. This conversion is carried out using the power converter unit between the source and the grid. Due to their adaptability in control and their low losses features, insulated gate bipolar transistors (IGBTs) are typically used for switching in the majority of power electronic inverters for grid connection [9]. The widely used renewable and green energy is shown with the VSI in Figure-4. The P-Q controller, an inverter, and a filter are the major components of the configuration. The filter helps to reduce the current harmonics produced by the PWM switching inverter. Based on a P-Q control strategy, the VSI will convert the DC form to usable AC power. The function of the controller is to determine the magnitude and angle of the voltage at the inverter terminal to ensure that the precise amount of electrical power from the source is transferred to the grid. The controller uses the decoupled voltage control method in the configuration, which is based on the d-q rotating frame. The configurations use two control loops, the outer voltage loop and the inner current loop, depicted in Figure-2 [10], and the controller is constructed in dq0 coordinates, allowing for the independent control of active and reactive power outputs. As demonstrated in Figure-4, the active power reference (Pref) and reactive power reference (Qref) settings of the inverter will determine how the DG unit operates. Each DG unit will function at its peak efficiency and ensure that there is no waste at the generation site by correctly managing Pref and Qref, as depicted in Figure-5.

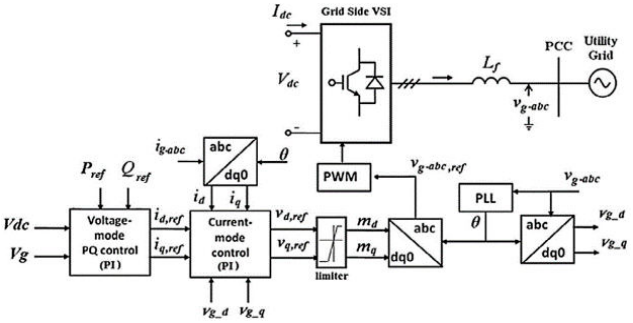

Figure-5. Two loops control of VSI.

Test system Description

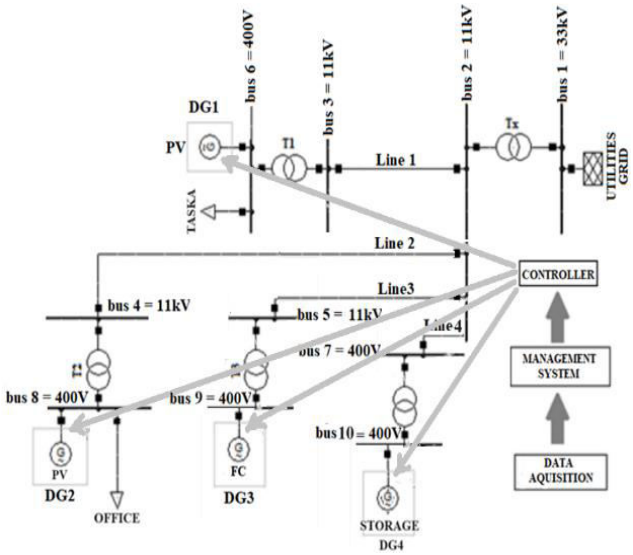

Figure-6. The typical distribution network is integrated with DG.

The suggested online management method is used with the usual distribution network shown in Figure-6 as an example. An external grid of 33 kV is fed into the test system model's radial distribution system, which has three identical DG units. The main substation transformers step down the power to 11 kV medium voltages. With a distribution line of π-line, the DG units are positioned 3 km apart. The system is supplied through three primary feeders, each of which has one DG unit and one type of load. Table-1 gives more information about the system under study.

Table-1. System model description.

Parameter	Description
External grid	• Grid represented by 33kV
Tx	• Transformer 33/11kV
T1, T2, T3 and T4	• Transformer 11/0.4kV
DG1 DG2	• Photovoltaic system
DG3	• Fuel cell system
DG4	• Battery storage system
Line 1, Line 2, Line 3 and Line 4	• 11kV with 3 km length

The distribution network is connected with highly advanced communication technology that connects the DG unit, grid, and loads, enabling the coordinated control between sources and loads. This creates a smart grid system with online capability. For a 24-hour operation, a data collecting device will scan the distribution network once each hour of load demand during a day. The data collecting device measures all load profiles, including active and reactive power requirements on the consumer's end, as well as the PV output power designated as DG1. The knowledge gained is put to use to control the DG units' future intervals of optimal operation. Every hour, the control system will determine the ideal set points for the DG units and remotely modify them over the communication link. According to Figure 6 there are two different types of loads engaged in this study: taska, office, and adjustable loads. Due to the electricity use during business hours, when people are typically engaged in human activities, office work, and commercial activities, a peak load occurs from 9 am to 6 pm every day. In this system, the power factor (PF) is set at 0.9 to prevent any more system losses, and the reactive power demand is modified by the current active power demand. A lower PF will make more current flow necessary, which will increase power loss. A distribution system's dependency on electrical power from the external grid is reduced when a group of DG units is permitted to inject active and reactive power into the system. This decreases losses and costs associated with the overall generation system. There will be five outputs and seven inputs for the suggested technique. The active and reactive powers of the loads, which are the adjusted load (PL1, QL1), office load (PL2, QL2), and commercial load (PL3, QL3), as well as the active power of the PV unit, will constitute the system's inputs. (PDG1). The system's outputs include the reactive power reference for DG1, DG2, DG3, and DG4 (Q DG1, Q DG2, DG3, and Q DG4) as well as the active power reference for DG3 and DG4 (PDG3, PDG4).

ANN Based Optimization of Active and Reactive Power of Inverter-Based DG

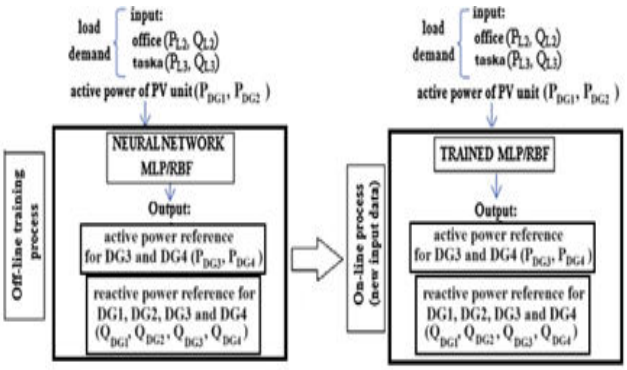

Figure-7. Description of inputs and outputs of the ANN.

The two-stage strategy based on the optimization process and ANN technology is the suggested method for managing the active and reactive power references of DG. The interior-point technique is used in the first stage of the optimization process to establish the ideal daily performance of DG units, as shown in Figure 7. Obtaining the load demand data and photovoltaic (PV) output power as the optimization's inputs is the initial stage before continuing with the process. The PV system is chosen as an input to the network, taking into account the PV intermittency difficulties brought on by the erratic weather conditions. Eight inputs are taken into account for the test system in this simulation instance, including the active and reactive load requirements of residential, office, and commercial loads, as well as the active power of DG1, which is the photovoltaic (PV) data. The optimal setting of DG units, which are the active power references of DG3 and DG4, as well as the reactive power references of DG1, DG2, DG3, and DG4, are determined by performing the optimization process using the interior-point algorithm. The objective function for the mathematical formulation of the optimal power flow is the minimization of total distribution network loss to solve the optimal reference power of the DG units, which is provided by,

$$\text{Min } P_{loss} = f(\boldsymbol{x}), \tag{5}$$

Dispatches from each DG unit are treated as the control variables in this study. The various constraints imposed on the optimization problem are described as follows:

i. All bus voltage limits:

$$u_{\min} \leq u_{t,i} \leq u_{\max}. \quad (6)$$

The voltage limit at the i-th node at t hour (ut, i) must be between the maximum and minimum output voltages of umin and umax.

ii. DG active power limits:

$$P_{\min} \leq P \leq P_{\max}. \quad (7)$$

Megawatt (MW) generation must be between the minimum and maximum active power limits Pmin and Pmax.

iii. DG reactive power limits:

$$Q_{\min} \leq Q \leq Q_{\max}. \quad (8)$$

Megavolt ampere reactive (MVAr) generation must be between the minimum and maximum reactive power limits Qmin and Qmax

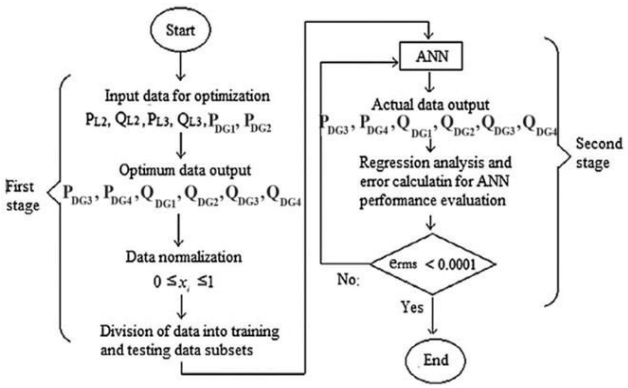

Figure-8. Summarize of the proposed system.

Implementation of ANN Using MATLAB

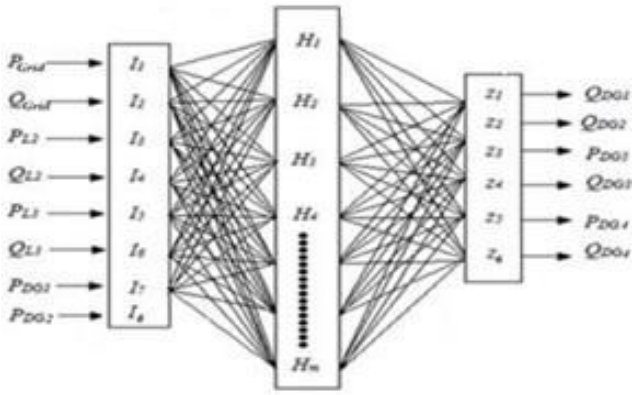

Figure-9. The three-layer architecture of MLP with different activation functions.

The neural network consists of two-layer feedforward networks with linear and sigmoid hidden neurons. In addition to the Levenberg-Marquardt backpropagation algorithm, its function is training. The next step is to choose the data that has been divided into two groups. The first stage of the management technique can be done after the inputs and outputs determination process. The active power reference for DG3 and DG4 (PDG3, PDG4), as well as the reactive power reference for DG1, DG2, DG3, and DG4 (Q DG1, Q DG2, Q DG3, and Q DG4), are output data from the optimization process that are gathered and used as target data for ANN models. Additionally, the office building (PL2, QL2), commercial building (PL3, QL3), and adjustable load (PL1, QL1) are the input data for the ANN, together with the active power of the PV unit.

The loaded data will then be split into three groups for training, validation, and testing, according to the values that have been set. Researchers claim that there is no method for defining the number of neurons. So, in this study, the default number of neurons is 10. Then ANN was chosen to receive training. The predicted values can be shown after the training. The time to anticipate the load values is then calculated by the ANN. If the predicted values were not satisfactory, the grid needed to be changed by increasing or decreasing the number of neurons.

The loaded data will then be split into three groups for training, validation, and testing, according to the values that have been set. Researchers claim that there is no method for defining the number of neurons. So, in this paper, the default number of neurons is 10. Then, ANN was chosen to receive training. The predicted values can be shown after the training. The time to anticipate the load values is then calculated by the ANN. If the predicted values were not satisfactory, the grid needed to be changed by increasing or decreasing the number of neurons.

The chosen data is then split into two groups; the first stage of the management technique can be carried out following the inputs and outputs determination process. The active power reference for DG3 and DG4 (PDG3, PDG4), as well as the reactive power reference for DG1, DG2, DG3, and DG4 (Q DG1, Q DG2, Q DG3, and Q DG4), are output data from the optimization process that are gathered and used as target data for ANN models. Additionally, the office building (PL2, QL2), commercial building (PL3, QL3), and adjustable load (PL1, QL1) are the input data for the ANN, together with the active power of the PV unit. With these parameters, the input data and target load were arbitrarily split into three categories: 70% were used for training data, 15% were used to validate data that the network is generalizing, and 0% were used to stop the training data before overfitting. A separate test of grid generalization was conducted using the final 15%. The number of concealed neurons will be counted as the next stage.

A network architectural model comprises three fundamental levels; the input layer is the top layer. The

concealed layer is found in the second layer. There is no relationship between the outward layer and the concealed layer. The third layer generates results. A 2-layer feedforward network with a sigmoid provides outputs and is the typical network used for pattern recognition.

Implementation of ANFIS Using MATLAB

In this study, ANFIS is used to anticipate various load values for power management models based on relevant inputs. The first stage of the management technique can be carried out following the inputs and outputs determination process. The active power reference for DG3 and DG4 (PDG3, PDG4), as well as the reactive power reference for DG1, DG2, DG3, and DG4 (Q DG1, Q DG2, Q DG3, and Q DG4), are output data from the optimization process that are gathered and used as target data for ANN models. Additionally, the office building (PL2, QL2), commercial (PL3, QL3), and adjustable load (PL1, QL1) are the input data for the ANN, together with the active power of the PV unit.

General information about a fuzzy inference system by the adaptive neuro-fuzzy inference system editor (FIS). The tool that displays and adjusts the membership functions connected to all variables, including input and output, is called a membership function editor. The four primary categories of the ANFIS editor are load data, produce FIS, train FIS, and test FIS. The effectiveness of the ANFIS models for data training, testing, and checking was assessed, and the optimal data set for training, testing, and checking was chosen based on the error.

Evaluation Metrics

In this study, the real power (P) and reactive power (Q) of the REDG system are altered at random to produce the training data for ANN and ANFIS. The evaluation forecasting metric has been used to evaluate ANN and ANFIS performance. The evaluation metrics of root mean square error (RMSE), mean absolute error (MAE), and mean absolute percent error (MAPE) are typically used to assess the effectiveness of the ANN and ANFIS, as was mentioned in the section on the research.

The root mean square error (RMSE) measures the discrepancy between calculated and projected values. The performance improves with a lower root mean square error (RMSE) value. The equation below can be used to determine root mean square error [11].

$$RMSE = \sqrt{\frac{1}{N}\sum_{i=1}^{N}(A-P)^2} \quad (9)$$

where
N = the total number of training data
A = the data on the x-axis (target values)
P = the data on the y-axis (prediction values)

The mean absolute error (MAE) measures the discrepancy between calculated and projected values. The performance improves with a lower mean absolute error (MAE) value. The equation below can be used to determine mean absolute error (MAE) [11].

$$\text{MAE} = \frac{1}{N}\sum_{i=1}^{N}(A-P) \quad (10)$$

where
N = the total number of training data
A = the data on the x-axis (target values)
P = the data on the y-axis (prediction values)

The mean absolute percent error (MAPE) measures the discrepancy between calculated and projected values. The performance improves with a lower mean absolute percent error (MAPE) value. The equation below can be used to determine mean absolute percent error (MAPE) [11].

$$\text{MAPE} = \frac{100}{N}\sum_{i=1}^{N}\frac{(A-P)}{P} \quad (11)$$

where
N = the total number of training data
A = the data on the x-axis (target values)
P = the data on the y-axis (prediction values)

Regression analysis is another method used to evaluate ANN and ANFIS performance in addition to evaluation metrics. To examine the relationship between two variables, regression analysis is frequently utilized. Regression analysis is utilized in this study to demonstrate the link between the goal and predicted values. The ANN or ANFIS performs better in regression analysis when the regression result is closer to 1. The equation below can be used to calculate the regression value, R2.

$$R^2 = 1 - \frac{\sum_{i=1}^{N}(A-P)^2}{\sum_{i=1}^{N}Ai^2} \quad (12)$$

where
N = the total number of training data
A = the data on the x-axis (target values)
P = the data on the y-axis (prediction values)

RESULTS AND DISCUSSIONS

Performance Comparison of the Developed ANN and ANFIS Battery Generation System.

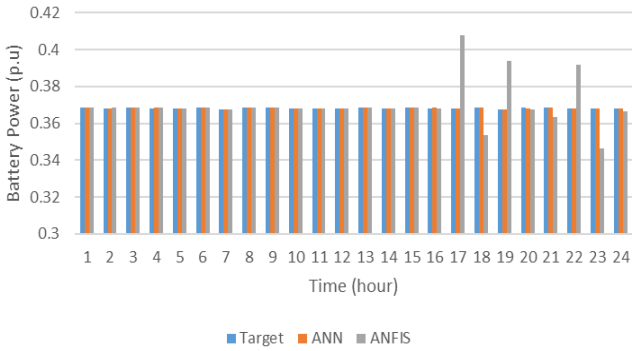

Figure-10. Battery output power ANN and ANFIS prediction vs target.

Figure-10 illustrates battery output power with a comparison of ANN, ANFIS, and Target data. The results indicate that ANN and ANFIS are considerably closer to the target data than ANFIS is, but that ANFIS is out of target data at times 17s, 19s, and 22s due to a high peak, whereas times 18s and 23s are lower. In other words, from 1 to 16, the ANN and ANFIS are near the target data. It demonstrates that every difference predicted by ANN is within a tolerable margin of error. It is conceivable to conclude that using the simulation ANN predicted is better and more appropriate for this project.

Figure-11 depicts the error for battery output power; ANN has better validation performance than ANFIS. Start time 1s to 16s shows almost close to the target data, but from 17s to 23s show the gap where the ANFIS error is out of the target data.

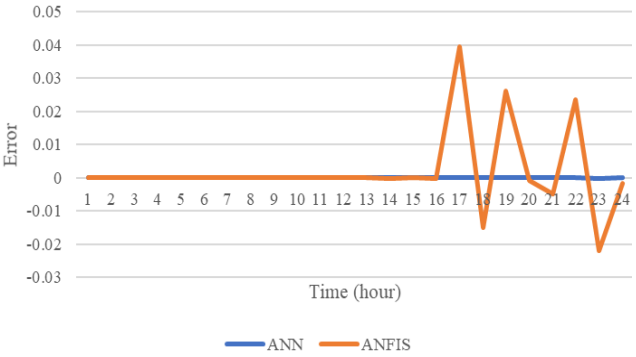

Figure-11. Error of battery output power ANN, ANFIS predicted vs target.

Figure-12 depicts a bar graph that compares Battery reactive power between ANN, ANFIS, and the target data. The results reveal that ANN and ANFIS are significantly closer to the target data; however, at times 17s, 19s, and 22s, ANFIS is out of the target data at a high peak, while at times 18s and 23s are lower. That is, from start time 1 to start time 16, the ANN and ANFIS are close to the target data. It demonstrates that all of the ANN-predicted differences are within a reasonable margin of error. It is possible to infer that using the simulation ANN predicted is more relevant and beneficial for this project.

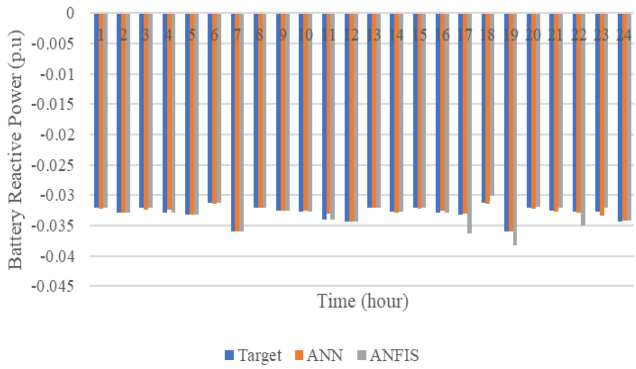

Figure-12. Battery reactive power ANN, ANFIS predicted vs target.

Figure-13 depicts the error for battery reactive power, with the best validation performance ANN compared to ANFIS. Start time 1s to 16s shows almost close to the target data, but from 17s to 23s show the gap where the ANFIS error is out of the target data.

Figure-13. Error of battery reactive power ANN, ANFIS predicted vs target.

Fuel Cell Generation System

Figure-14 depicts a bar graph that compares Fuel Cell output power between ANN and ANFIS versus to Target data. Results show that ANN and ANFIS are much closer to the target data; however, at times 17s, 19s, and 22s, ANFIS is out of the target data at a high peak, while times 18s and 23s are lower. That is, from start time 1 to start time 16, the ANN and ANFIS are close to the target data. It demonstrates that all the ANN-predicted differences are within a reasonable margin of error. It is possible to infer that using the simulation ANN predicted is more relevant and beneficial for this project.

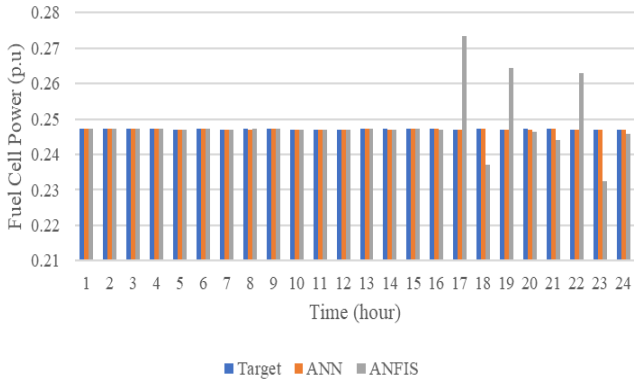

Figure-14. Fuel cell output power ANN, ANFIS predicted vs target.

Figure-15 depicts the error for Fuel Cell output power, with the best validation performance being ANN compared to ANFIS. Start time 1s to 16s shows almost close to the target data, but from 17s to 23s shows a gap where the ANFIS error is out of the target data.

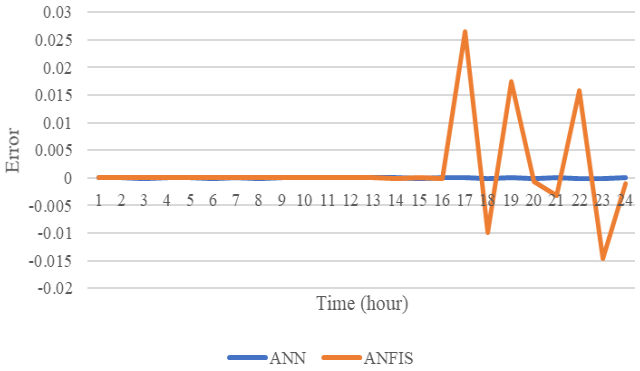

Figure-15. Error of fuel cell output power ANN, ANFIS predicted vs target.

Figure-16 depicts a bar graph that compares the Fuel Cell reactive output power between ANN, ANFIS, and Target data. The results reveal that ANN and ANFIS are significantly closer to the target data; however, at times 6s, 16s, 18s, and 20s, ANFIS is out of the target data at a high peak, while times 17s are lower. That is, from start time 1 to start time 16, the ANN and ANFIS are close to the target data. It demonstrates that all the ANN-predicted differences are within a reasonable margin of error. It is possible to infer that using the simulation ANN predicted is more relevant and beneficial for this project.

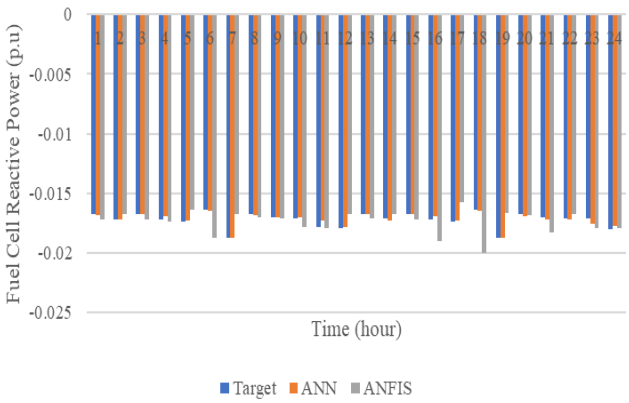

Figure-16. Fuel cell reactive power ANN, ANFIS predicted vs target.

Figure-17 depicts the error for Fuel Cell reactive power, with the best validation performance being ANN compared to ANFIS. Start time 1s to 16s shows almost close to the target data, but from 17s to 23s shows a gap where the ANFIS error is out of the target data.

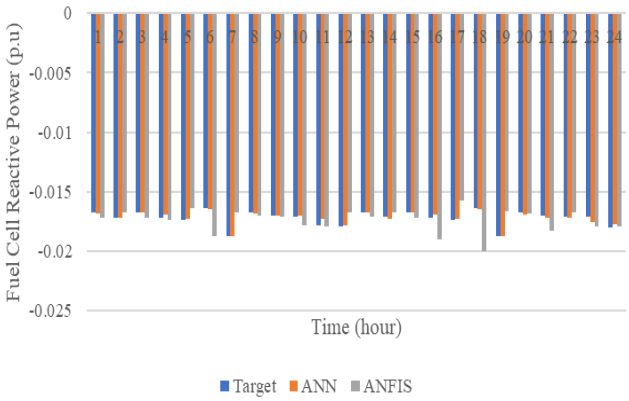

Figure-17. Error of fuel cell reactive power ANN, ANFIS predicted vs target.

Photovoltaic 1-Generation System

Figure-18 depicts a bar graph that compares PV1 reactive power between ANN, ANFIS, and Target data. The results reveal that ANN and ANFIS are significantly closer to the target data; however, at times 17s, 19s, and 22s, ANFIS is out of the target data at a high peak, while at times 18s and 23s are lower. That is, from start time 1 to start time 16, the ANN and ANFIS are close to the target data. It shows that almost all ANN-predicted differences are within a reasonable margin of error. It is possible to infer that using the simulation ANN predicted is more relevant and beneficial for this project.

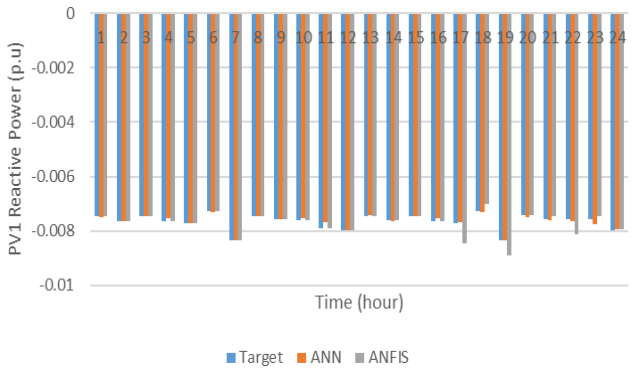

Figure-18. PV1 reactive power ANN, ANFIS predicted vs target.

Figure-19 depicts the error for PV1 reactive power, with the best validation performance being ANN compared to ANFIS. Start time 1s to 16s shows almost close to the target data, but from 17s to 23s shows a gap where the ANFIS error is out of the target data.

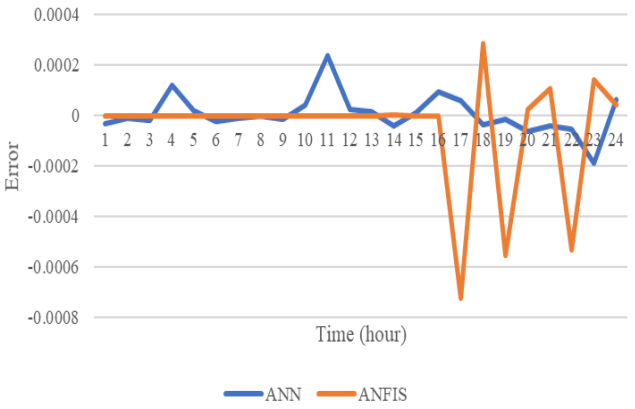

Figure-19. Error of PV1 reactive power ANN, ANFIS predicted vs target.

Photovoltaic 2-Generation System

Figure-20 depicts a bar graph that compares PV2 reactive power between ANN, ANFIS, and Target data. The results reveal that ANN and ANFIS are significantly closer to the target data; however, at times 17s, 19s, and 22s, ANFIS is out of the target data at a high peak, while at times 18s and 23s are lower. That is, from start time 1 to start time 16, the ANN and ANFIS are close to the target data. It demonstrates that all of the ANN-predicted differences are within a reasonable margin of error. It is possible to infer that using the simulation ANN predicted is more relevant and beneficial for this project.

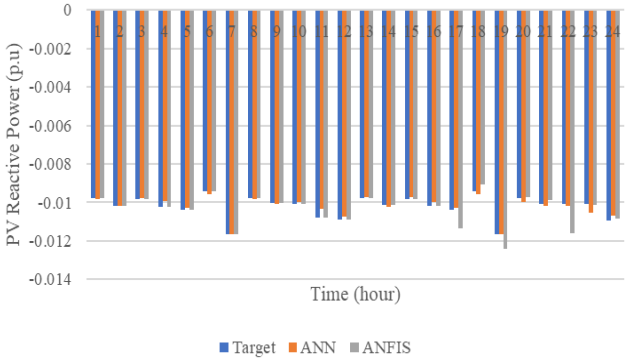

Figure-20. PV2 reactive power ANN, ANFIS predicted vs target.

Figure-21 depicts the error for error PV2 reactive power, with the best validation performance being ANN compared to ANFIS. Start time 1s to 16s shows almost close to the target data, but from 17s to 23s shows a gap where the ANFIS error is out of the target data.

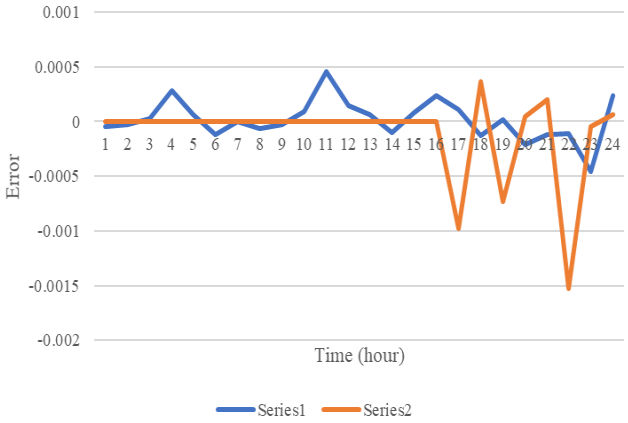

Figure-21. Error of PV2 reactive power ANN, ANFIS predicted vs target.

Result of Evaluation Performance Comparison of the Developed ANN and ANFIS

The evaluation of performance comparison of ANN and ANFIS is calculated by coefficient of determination, root mean square error (RMSE), mean absolute error (MAE), and mean absolute percentage error (MAPE) as shown in Table 2 to Table-6. The comparative analysis shows that the error of ANN active power for the battery and fuel cell, and reactive power for the battery, fuel cell, and PV2, delivers the minimum deviation compared to ANFIS from the predicted data. The result showed that the R2, root mean square error (RMSE), mean absolute error (MAE), and mean absolute percentage error (MAPE) values of the constructed models for ANN predicted are more exact in closing the target, where the error is minor as compared to ANFIS predicted.

Table-2. Evaluation of performance comparison for the active power of the battery.

Model	ANN	ANFIS
R^2	1.60349E-14	8.3158E-12
RMSE	5.85896E-05	0.012102896
MAE	9.09078E-06	0.001880242
MAPE	0.011714474	1.455235337

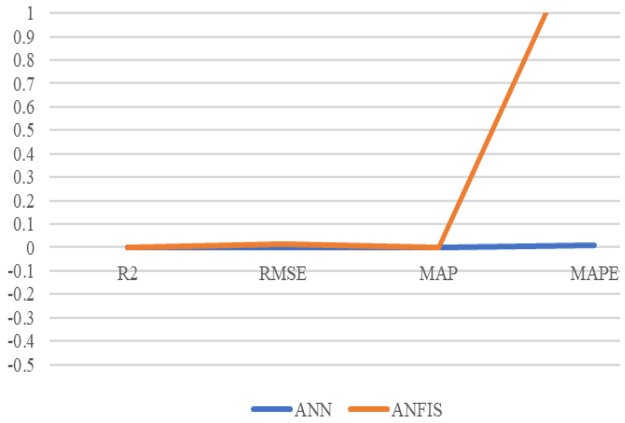

Figure-22. Evaluation of performance comparison for the active power of the battery.

Table-2 and Figure-22 show the evaluation Performance Comparison of Active Power Battery topology was the most effective predicted outcome between ANN and ANFIS. The values obtained from ANN analysis for R^2 and MAPE were 1.60349E-14 and 0.011714474, while for RMSE and MAE values were 9.09078E-06 and 0.011714474. These results indicated that the prediction accuracy of the ANN was better than the ANFIS analysis for the effectiveness of the predictive result.

Table-3. Evaluation of performance comparison for the reactive power of the battery.

Model	ANN	ANFIS
R^2	1.8032E-11	3.65E-11
RMSE	0.00031611	0.000973
MAE	8.7668E-06	-0.00022
MAPE	-0.609694	-1.23392

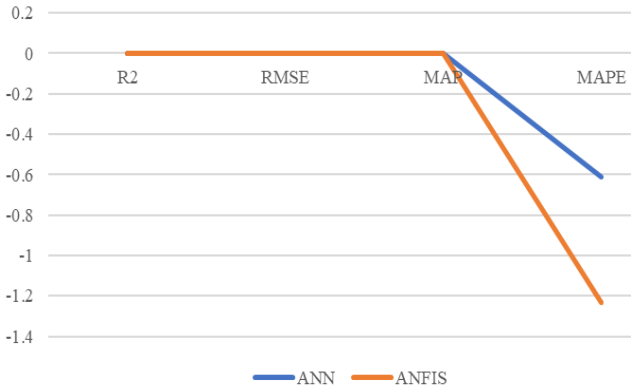

Figure-23. Evaluation of performance comparison for the reactive power of the battery.

Table-3 and Figure-23 show the evaluation performance comparison of reactive power. Battery topology was the most effective in terms of predictive results between ANN and ANFIS. The values obtained from ANN analysis for R^2 and MAPE values were 1.8032E-11and -0.609694, while for RMSE and MAE values were 0.00031611 and 8.7668E-06. These results indicated that the prediction accuracy of the ANN was better than the ANFIS analysis for the effectiveness of the predictive result.

Table-4. Evaluation of performance comparison for the active power of the fuel cell.

Model	ANN	ANFIS
R^2	5.88931E-16	7.28169E-13
RMSE	4.12762E-05	0.008113456
MAE	-5.80133E-06	0.001262203
MAPE	0.013430046	1.453871773

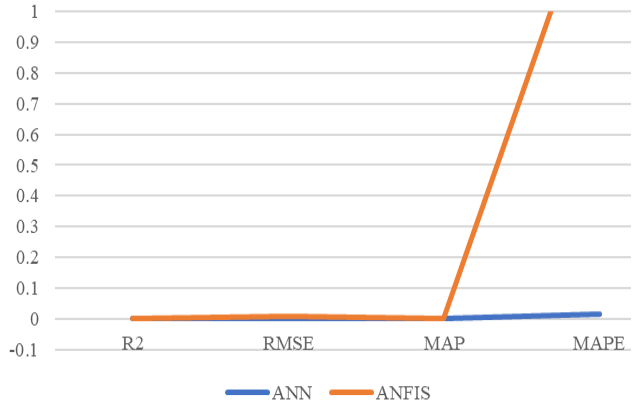

Figure-24. Evaluation of performance comparison for the active power of the fuel cell.

Table-4 and Figure-24 show the evaluation performance comparison of active power Fuel Cell topology was the most effective in terms of predictive result between ANN and ANFIS. The values obtained

from ANN analysis for R^2 and MAPE were 5.88931E-16 and 0.013430046, while for RMSE and MAE were 4.12762E-05 and -5.80133E-06. These results indicated that the prediction accuracy of the ANN was better than the ANFIS analysis for the effectiveness of the predictive result.

Table-5. Evaluation of performance comparison for the reactive power of the fuel cell.

Model	ANN	ANFIS
R^2	1.3832E-12	6.06E-13
RMSE	0.00018799	0.001275
MAE	1.9039E-05	-0.00016
MAPE	-0.802295	-5.15661

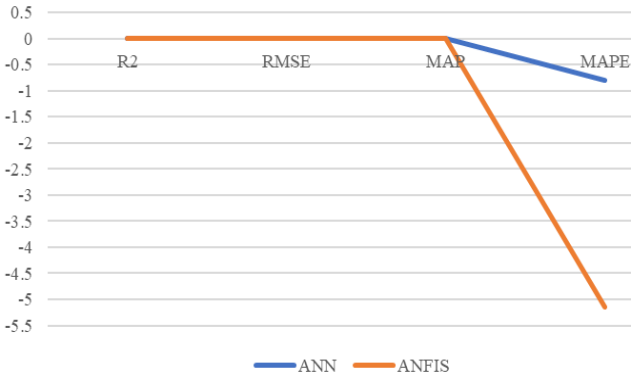

Figure-25. Evaluation of performance comparison for the reactive power of the fuel cell.

Table-5 and Figure-25 show the evaluation performance comparison of the reactive power Fuel Cell topology was the most effective in terms of predictive results between ANN and ANFIS. The data obtained from ANN analysis for R^2 and MAPE values were 1.3832E-12 and -0.802295, while for RMSE and MAE values were 0.00018799and 1.9039E-05. These results indicated that the prediction accuracy of the ANN was better than the ANFIS analysis for the effectiveness of the predictive result.

Table-6. Evaluation of performance comparison for the reactive power of PV1.

Model	ANN	ANFIS
R^2	5.16355E-14	1.00798E-13
RMSE	7.58629E-05	0.000225941
MAE	6.71329E-06	-5.0154E-05
MAPE	-0.666237745	-1.236686263

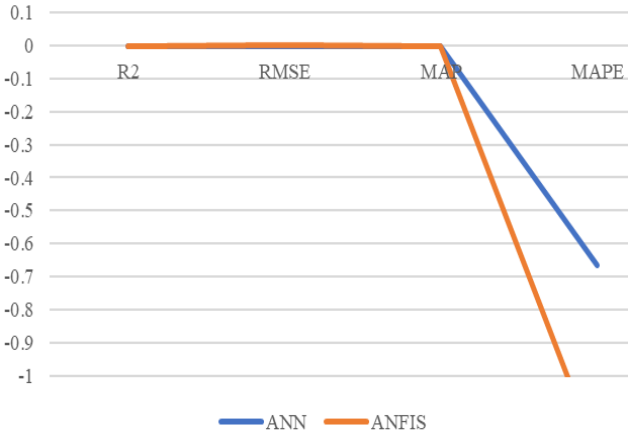

Figure-26. Evaluation of performance comparison for the reactive power of PV1.

Table-6 and Figure-26 show the evaluation performance comparison of the reactive power PV1 topology was the most effective in predictive results between ANN and ANFIS. The data obtained from ANN analysis for R^2 and MAPE values were 5.16355E-14 and -0.666237745, while for RMSE and MAE values were 7.58629E-05 and 6.71329E-06. These results indicated that the prediction accuracy of the ANN was better than the ANFIS analysis for the effectiveness of the predictive result.

Table-7. Evaluation of performance comparison for the reactive power of PV2.

Model	ANN	ANFIS
R^2	1.0781E-12	1.47E-12
RMSE	0.00018067	0.000409
MAE	1.683E-05	-0.00011
MAPE	-1.3576828	-1.5336

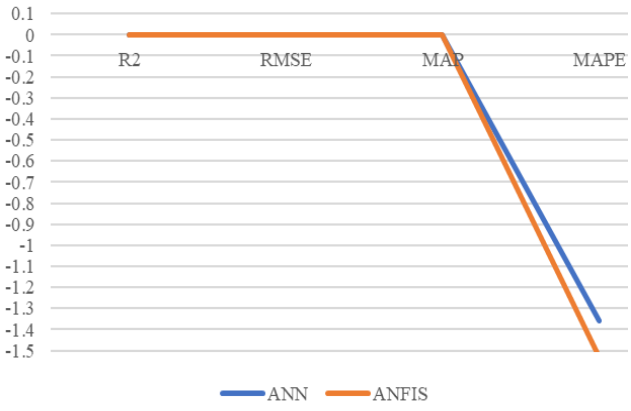

Figure-27. Evaluation of performance comparison for the reactive power of PV2.

Table-7 and Figure-27 show the evaluation performance comparison of the reactive power PV2

topology was the most effective in predictive results between ANN and ANFIS. The data obtained from ANN analysis for R^2 and MAPE values were 1.0781E-12 and -1.3576828, while for RMSE and MAE values were 0.00018067 and 1.683E-05. These results indicated that the prediction accuracy of the ANN was better than the ANFIS analysis for the effectiveness of the predictive result.

CONCLUSIONS

Dynamic models of three types of renewable and green energy resources have been developed in MATLAB/Simulink/SimPowerSystems, which include a Photovoltaic generation system, a fuel cell generation system, and a battery energy storage system. In the development of dynamic models, two modeling techniques are used based on the detail and phasor models. In the detailed model, the switching of power electronics devices and other physical components is considered. Since the detailed model consumes a long computational time to simulate, it is used for studying harmonics during steady state operation and other studies involving a small number of renewable and green energy resources. On the other hand, the simplified phasor model is used to reduce the simulation time when performing power system studies in a network with many renewable and green energy resources. The developed models' performances are compared to the reported performance in the literature, and the results are found to be comparable.

This project has also successfully developed an intelligent microgrid central controller for online management of power contributed by a group of renewable and green energy resources. An ANN and ANFIS are used to replace the task of the optimization process in finding the optimal operating point of renewable and green energy resources in the test microgrid system. There are two stages involved in the development of the intelligent microgrid central controller: optimal power flow analysis and construction of ANN and ANFIS. The database is first obtained from optimal power flow simulations using the DIgSILENT software, and then, it is used to train an ANN and ANFIS to predict the optimal power from each energy resource available in the network. The technique's effectiveness is shown on the test microgrid system with three renewable and green energy resources. The simulation results indicate that an ANN based controller is effective in predicting the optimal power operating point between the time steps used in the optimal power flow simulations. This predictive control technique is suitable to be integration into a microgrid system in which more realistic forecasted inputs are available.

ACKNOWLEDGMENT

We wish to express our gratitude to the honorable Universiti Teknikal Malaysia Melaka and special appreciation and gratitude, especially for the Faculty of Electrical Technology and Engineering (FTKE) and Energy and Smart Grid Technology Research Group (ESGIT), Center for Robotics and Industrial Automation (CERIA), for supporting this research.

REFERENCES

[1] T. Hoang *et al*. 2021. Integrating renewable sources into the energy system for a smart city as a sagacious strategy towards a clean and sustainable process. Journal of Cleaner Production. 305: 127161.

[2] M. A. Bagherian and K. Mehranzamir. 2020. A comprehensive review of renewable energy integration for combined heat and power production. Energy Conversion and Management. 224: 113454.

[3] M. McPherson and B. Stoll. 2020. Demand response for variable renewable energy integration: A proposed approach and its impacts. Energy. 197: 117205.

[4] Ali Q. Al-Shetwi *et al*. 2020. Grid-connected renewable energy sources: Review of the recent integration requirements and control methods. Journal of Cleaner Production. 253: 119831.

[5] N. T. Mbungu *et al*. 2020. An overview of renewable energy resources and grid integration for commercial building applications. Journal of Energy Storage. 29: 101385.

[6] R. M. Elavarasan *et al*. 2020. A Comprehensive Review on Renewable Energy Development, Challenges, and Policies of Leading Indian States with an International Perspective. IEEE Access. 8: 74432-74457.

[7] R. Alizadeh *et al*. 2020. Improving renewable energy policy planning and decision-making through a hybrid MCDM method. Energy Policy. 137: 111174.

[8] L. Li *et al*. 2022. Review and outlook on the international renewable energy development. Energy and Built Environment. 3(2): 139-157.

[9] T. E.-Eriksen *et al*. 2021. Hydrogen-based systems for integration of renewable energy in power systems: Achievements and perspectives. International Journal of Hydrogen Energy. 46(63): 31963-31983.

[10] P. Hu *et al*. 2023. Inertia estimation of a renewable-energy-dominated power system. Renewable and Sustainable Energy Reviews. 183: 113481.

[11] Y. Xu *et al*. 2022. Blockchain-Based Trustworthy Energy Dispatching Approach for High Renewable Energy Penetrated Power Systems. IEEE Internet of Things Journal. 9(12): 10036-10047.

[12] S. Impram *et al*. 2020. Challenges of renewable energy penetration on power system flexibility: A survey. Energy Strategy Reviews. 31: 100539.

[13] S. Yang *et al*. 2021. A Graph-Based Method for Vulnerability Analysis of Renewable Energy Integrated Power Systems to Cascading Failures. Reliability Engineering & System Safety. 207: 107354.

[14] A. Elmelegi *et al*. 2021. Optimized Tilt Fractional Order Cooperative Controllers for Preserving Frequency Stability in Renewable Energy-Based Power Systems. IEEE Access. 9: 8261-8277.

[15] Y. Zhou *et al*. 2021. Real-time cost-minimization power-allocating strategy via model predictive control for fuel cell hybrid electric vehicles. Energy Conversion and Management. 229: 113721.

[16] D. F. Pereira *et al*. 2021. Nonlinear Model Predictive Control for the Energy Management of Fuel Cell Hybrid Electric Vehicles in Real Time. IEEE Transactions on Industrial Electronics. 68(4): 3213-3223.

[17] H. He *et al*. 2020. Model Predictive Control with Lifetime Constraints-Based Energy Management Strategy for Proton Exchange Membrane Fuel Cell Hybrid Power Systems. IEEE Transactions on Industrial Electronics. 67(10): 9012-9023.

[18] J. Xu *et al*. 2020. Modelling and control of vehicle vehicle-integrated thermal management system of a PEM fuel cell vehicle. Energy. 199: 117495.

[19] L. Sun *et al*. 2020. Active disturbance rejection temperature control of open-cathode proton exchange membrane fuel cell. Applied Energy. 261: 114381.

[20] W. Chaichan *et al*. 2022. Optimization of stand-alone and grid-connected hybrid solar/wind/fuel cell power generation for green islands: Application to Koh Samui, southern Thailand. Energy Reports, 8: 480-493, doi: 10.1016/j.egyr.2022.07.024

[21] K. Das *et al*. 2021. Techno-economic optimisation of stand-alone hybrid renewable energy systems for concurrently meeting electric and heating demand. Sustainable Cities and Society. 68: 102763.

[22] K. Das, *et al*. 2021. Impact of storage technologies, temporal resolution, and PV tracking on stand-alone hybrid renewable energy for an Australian remote area application. Renewable Energy. 173: 362-380.

[23] F. Akram *et al*. 2020. Techno-economic optimization analysis of a stand-alone renewable energy system for remote areas. Sustainable Energy Technologies and Assessments. 38: 100673.

[24] M. H. Saeed *et al*. 2021. A Review on Microgrids' Challenges & Perspectives. IEEE Access. 9: 166502-166517.

[25] W. Tushar *et al*. 2021. Peer-to-peer energy systems for connected communities: A review of recent advances and emerging challenges. Applied Energy. 282: 116131.

[26] S. R. Sinsel *et al*. 2020. Challenges and solution technologies for the integration of variable renewable energy sources review. Renewable Energy. 145: 2271-2285.